Effect of Al$_2$O$_3$ Nanoparticles as Reinforcement on the Tensile Behavior of Al-12Si Composites

Pan Ma [1], **Yandong Jia** [2,*], **Prashanth Konda Gokuldoss** [3,4,*] iD , **Zhishui Yu** [1], **Shanglei Yang** [1], **Jian Zhao** [1] **and Chonggui Li** [1]

[1] School of Materials Engineering, Shanghai University of Engineering Science, 201620 Shanghai, China; mapanhit@hotmail.com (P.M.); yuzhishui@sues.edu.cn (Z.Y.); yslei@126.com (S.Y.); zhaojianhit@163.com (J.Z.); chongguili@sues.edu.cn (C.L.)
[2] School of Materials Science and Engineering, Shanghai University, 200444 Shanghai, China
[3] Department of Manufacturing and Civil Engineering, Norwegian University of Science and Technology, 222815 Gjøvik, Norway
[4] Erich Schmid Institute of Materials Science, Austrian Academy of Sciences, A-8700 Leoben, Austria
[*] Correspondence: yandongjia@shu.edu.cn (Y.J.); kgprashanth@gmail.com (P.K.G.); Tel.: +86-137-6107-8756 (Y.J.); +47-973-646-67 (P.K.G.)

Abstract: Al$_2$O$_3$ nanoparticle-reinforced Al-12Si matrix composites were successfully fabricated by hot pressing and subsequent hot extrusion. The influence of weight fraction of Al$_2$O$_3$ particles on the microstructure, mechanical properties, and the corresponding strengthening mechanisms were investigated in detail. The Al$_2$O$_3$ particles are uniformly distributed in the matrix, when 2 and 5 wt. % of Al$_2$O$_3$ particles were added to the Al-12Si matrix. Significant agglomeration can be found in composites with 10 wt. % addition of Al$_2$O$_3$ nanoparticles. The maximum hardness, the yield strength, and tensile strength were obtained for the composite with 5 wt. % Al$_2$O$_3$ addition, which showed an increase of about ~11%, 23%, and 26%, respectively, compared with the Al-12Si matrix. Meanwhile, the elongation increased to about ~30%. The contribution of different mechanisms including Orowan strengthening, thermal mismatch strengthening, and load transfer strengthening were analyzed. It was shown that the thermal mismatch strengthening has a more significant contribution to strengthening these composites than the Orowan and load transfer strengthening mechanisms.

Keywords: Al metal matrix composites; microstructure; mechanical properties; strengthening mechanism

1. Introduction

Al metal matrix composites (MMCs) have gained considerable attention as the ideal candidates for potential lightweight materials used in automobiles and other structural applications because of their attractive properties, such as low density, high specific stiffness, and superior wear resistance [1–6]. Recently, nano-sized reinforcements have been examined for the fabrication of Al-based composites. It has been shown that the addition of a small amount of fine ceramic particles improves the strength significantly [7,8]. Al$_2$O$_3$ particles with high specific stiffness and superior high temperature properties are used as inert ceramic reinforcement phases in MMCs [9,10]. A large number of studies have been performed on the fabrication and characterization of nano-sized Al$_2$O$_3$-reinforced Al matrix composites. Karbalaei Akbari et al. [11] studied nano-sized Al$_2$O$_3$-reinforced A356 alloy with stirring casting, and agglomerated nanoparticles were observed on dendrites in the fracture surface of the Al-Al$_2$O$_3$ reinforcement samples. Su et al. [12] fabricated Al$_2$O$_3$ nanocomposites by solid-liquid mixed casting combined with ultrasonic treatment and demonstrated that the ultrasonic vibration during the solidification was beneficial to refine the grain structure, and to improve the resulting distribution

of Al_2O_3 nanoparticle in the matrix. Sajjadi et al. [13,14] showed that decreasing the alumina particle size combined with compo-casting process can yield the best mechanical properties for Al-Al_2O_3 composites. The addition of alumina led to the improvement in yield strength (YS), ultimate tensile strength (UTS), compression strength, and hardness. However, the poor wettability of Al_2O_3 with molten aluminum makes it difficult to achieve a uniform distribution of Al_2O_3 nanoparticles in the composite [15].

The results demonstrate that the solidification processes have some advantages such as a wide selection of materials and range of materials that can be processed. Good matrix-particle bonding, ease in controlling the microstructure of the matrix, and flexibility in processing are some attractive features. However, the solidification processes are not suited for the dispersion of fine-sized particles due to the possibility of the formation of agglomeration. Agglomerate formation is due to the van der Waals force of attraction, non-uniform particle distribution, and poor wettability at the interface between metallic and ceramic reinforcements [16–22]. Powder metallurgy (PM) is an alternative fabrication technique the can yield a uniform distribution of reinforcement and flexibility in reinforcement composition and design [18–22]. Al matrix composites reinforced with nano- and submicron-sized Al_2O_3 particles were prepared by wet attrition milling and subsequent hot extrusion processing by Tabandeh Khorshid et al. [23]. It has been observed that both the hardness and strength of the composites increase and reach a saturation before showing a decline upon increasing the volume fraction of the nanoparticles. Razavi et al. [24] addressed the effect of mechanical milling and reinforcement nanoparticles on the densification response and the compressibility of aluminum powder. However, the effect of reinforcement on the strengthening mechanisms are not well illustrated. To facilitate the development of such composites, it is necessary to fully understand the strengthening mechanism of nano-sized particle reinforcements in the Al matrix composite. In this paper, the nano Al_2O_3 particle-reinforced Al-12Si matrix composites were prepared by powder metallurgy. Al-12Si alloy was chosen for this study because it is a near eutectic composition with good fluidity that has been widely used for a variety of industrial applications [25–28]. The influence of the weight fraction of Al_2O_3 particles on the microstructure and mechanical properties of Al alloy matrix was studied in detail. Additionally, the strengthening mechanism operating in these materials was investigated.

2. Materials and Methods

The Al-12Si gas atomized alloy powder (nominal composition of Al-88 wt. % and Si-12 wt. %) was selected as the matrix material. Al_2O_3 nanoparticles (d50 ~50 nm) of 2%, 5%, and 10% wt. % were used as reinforcement. The powders were milled to have a uniform mixture of reinforcement in the Al-12Si matrix. Milling was performed in a planetary ball mill (Retsch, Haan, Germany) under an argon atmosphere at room temperature for 2 h. The milling speed and ball to powder ratio were 150 rpm and 10:1, respectively. Consolidation (hot pressing) of the homogeneously mixed powders were carried out using hardened steel dies. Samples with a diameter of 10 mm and a height of 10 mm were hot pressed using the following parameters: load—600 MPa, temperature—673 K, and time—15 min. The samples were subsequently hot extruded with a pressure of ~800 MPa at 673 K, and the extrusion ratio was 6:1. As a result, 4-mm diameter rods were obtained after hot extrusion. For comparison, a monolithic Al-12Si matrix alloy (without reinforcement) was also fabricated by the same method.

For metallographic observation, the samples were prepared using conventional grinding and polishing techniques (from 200 grit to 4000 grit papers and then cloth polishing using diamond paste). The samples were then etched in 0.5% Hydroflouricacid (HF) solution. The microstructure of the composites were characterized by optical microscope (OM) and scanning electron microscope (SEM, Gemini1530 Zeiss) - (Carl Zeiss AG, Oberkochen, Germany). The structural characterization was performed by X-ray diffraction using D3290 PANalytical X'pert PRO (Almelo, The Netherlands) equipped with Cu-Kα radiation. Hardness measurements were carried out using a Vickers micro-hardness (Schimadzu, Dusiburg, Germany) tester at a constant load of 200 gf for a dwell time of 15 s. Tensile tests were carried out using an Instron-5869 device (INSTRON GmbH, Darmstadt,

Germany) at a rate of 0.5 mm/min, and the strain was calculated using a laser extensometer. The tensile test samples (according to American Society of Testing and Materials (ASTM) standard: ASTM: E8/E8M–13a) were cylindrical tensile bars with a total length of 52 mm that were machined from the extruded samples. The dimensions along the gauge length of the tensile bars were: length—17.5 mm, diameter—3.5 mm, and 4 mm around the grips. Three nominally identical specimens were tested to obtain the average values.

3. Results

3.1. Microstructure Analysis and Phase Identification

SEM micrographs of monolithic Al-12Si and Al-12Si/Al_2O_3 nanocomposites are shown in Figure 1. The extruded sample in Figure 1a reveals that the eutectic Si (~20 μm) is uniformly distributed in the Al matrix. Figure 1b,c show the microstructure of the composites as a function of the increasing content of Al_2O_3 particles. It can be observed from Figure 1b,c that the Al_2O_3 particles have a relative homogeneous distribution without significant agglomeration of the particles. When the reinforcement content reaches 10 wt. %, the agglomeration of the Al_2O_3 particles is quite evident (Figure 1d). The degree of Al_2O_3 agglomeration varies randomly throughout the samples, as marked in the Figure 1d, which may lead to the formation of defects such as pores and may act as stress concentrators, thereby hampering the overall properties of the composites. The high magnification image in Figure 2a shows the presence of agglomeration in the Al-12Si/Al_2O_3 (10 wt. %) nanocomposite. The energy dispersive spectrum analysis (Figure 2b) shows that the small particles within the agglomeration consist mainly of Al and O and the ratio is close to that of Al_2O_3. Since the nanoparticles have high surface energy due to the high surface to volume ratio, the nanoparticles tend to stick with each other and form agglomerates. Hence, the agglomerates increase with greater additions of the nanoparticles (in excess), resulting in an uneven distribution of the reinforcement in the matrix. Nevertheless, no visible flaws or pores were observed at the Al_2O_3/Al interface.
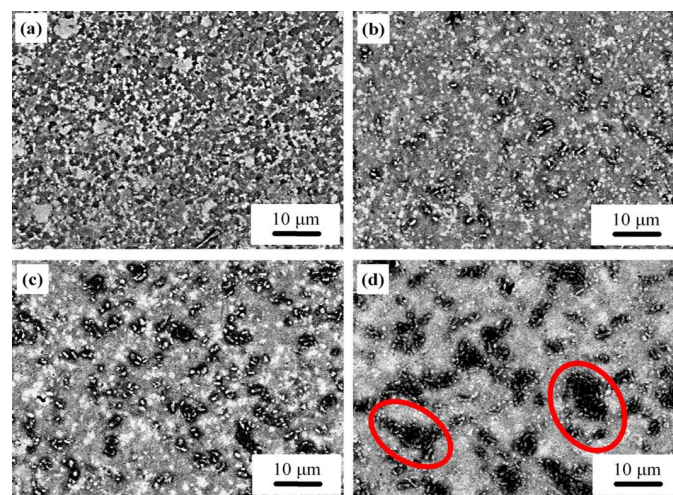

Figure 1. Scanning Electron Microscopy (SEM) images of hot extruded Al-12Si/Al_2O_3 nanocomposites with (**a**) 0, (**b**) 2, (**c**) 5, and (**d**) 10 wt. % reinforcement.

Figure 3 shows the XRD pattern of the composites reinforced with different contents of Al2O3. As observed, the samples mainly consist of three phases: (1) the Al matrix phase; (2) the Si phase from the matrix; and (3) the Al_2O_3 phase from the reinforcement. The diffraction peaks of the Al phase show the highest intensity because of their weight fraction in the composite. At 2 wt. % Al_2O_3 content, the diffraction peaks of v are hard to observe in the XRD pattern due to their low intensity. When the Al_2O_3 content increases to 5 wt. %, the small diffraction peaks of the Al_2O_3 phase are visible, and

their intensity increases when the Al_2O_3 content is increased to 10 wt. %. No other visible peaks were observed, suggesting that there is no additional phase formed between the (Al-12Si) matrix and the (Al_2O_3) reinforcement.
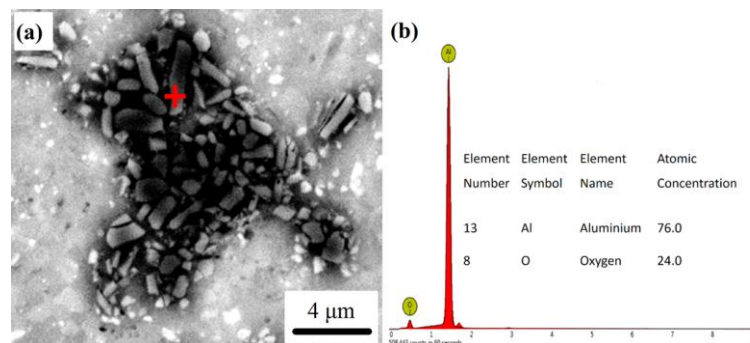

Figure 2. Scanning Electron Microscopy (SEM) image and Energy Dispersive Spectroscopy (EDS) analysis data for Al-12Si/10 wt. % Al_2O_3 nanocomposite in the as-extruded condition.
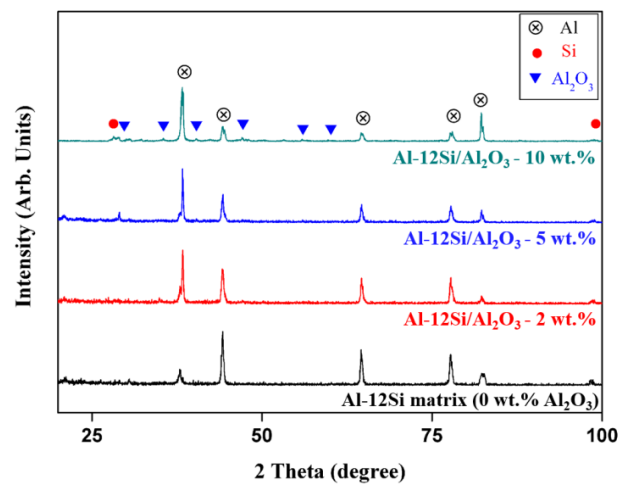

Figure 3. XRD analysis of Al-12Si/Al_2O_3 nanocomposites with (**a**) 0, (**b**) 2, (**c**) 5, and (**d**) 10 wt. % addition of Al_2O_3 reinforcement.

3.2. Physical and Mechanical Properties

Both the theoretical and experimental densities for all composite samples are listed in Table 1. The theoretical density of the composites are calculated using the rule of mixtures. High relative densities are achieved for all composites, indicating a good interface between the Al-Si matrix and the Al_2O_3 reinforcement. The relative density for the composite with 10 wt. % Al_2O_3 decreases slightly due to the agglomeration of Al_2O_3 particles, which leads to the presence of some pores.

Table 1. Density of the as-extruded Al-12Si/Al_2O_3 nanocomposites.

Weight Percent of Al_2O_3 (%)	Theoretical Density (g/cc)	Measured Density (g/cc)	Relative Density (%)
0	2.61	2.60	99.6
2	2.63	2.61	99.2
5	2.66	2.64	99.5
10	2.70	2.65	98.1

Figure 4 shows the Vickers hardness data for the Al-12Si/Al_2O_3 nanocomposites. The matrix shows a hardness value of 72 ± 1 $HV_{0.2}$, which increases to 77 ± 1 $HV_{0.2}$ (a change of ~5 $HV_{0.2}$)

when 2 wt. % of Al_2O_3 reinforcement is added to the matrix. The composite reinforced with 5 wt. % Al_2O_3 nanoparticles shows a higher hardness (80 ± 1 $HV_{0.2}$) compared to the other systems. With a further increase in the weight percentage of Al_2O_3 nanoparticles (to 10 wt. %), the composites show a decrease in the hardness value compared to the former ones due to the porosity and irregularities generated by the agglomeration of nanoparticles. Al_2O_3 nanoparticles dispersed uniformly in the Al-12Si alloy may significantly improve their hardness properties compared to the base alloy. The hard Al_2O_3 nanoparticles in the Al matrix act as barriers to the motion of dislocations generated in the matrix and the higher particle density causes Orowan mechanism. However, an increased addition of nanoparticles leads to agglomeration of the reinforcement, resulting in an increased level of porosity in the material and a subsequent degradation of the hardness values.
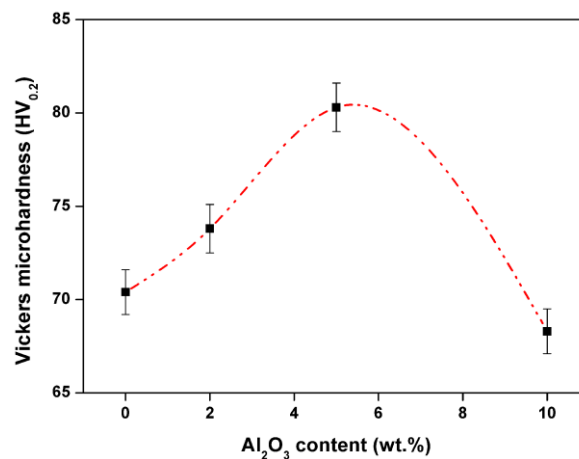

Figure 4. Vickers hardness measurements of Al-12Si/Al_2O_3 nanocomposites produced by the hot extrusion method.

Figure 5 shows the room temperature tensile stress-strain curves of the nanocomposite, and their properties are summarized in Table 2. It can be observed that the addition of Al_2O_3 significantly improves the yield strength (YS), ultimate tensile strength (UTS), and elongation of the Al-12Si matrix up to 5 wt. % Al_2O_3 addition. This is due to the good dispersion and strong interfacial bonding between the Al-12Si matrix and Al_2O_3 reinforcement. The YS, UTS, and elongation of the Al-12Si matrix in the as-extruded condition is found to be 198 MPa, 228 MPa, and 23%, respectively. Adding 2 wt. % of Al_2O_3 changes the YS, UTS, and elongation to 228 MPa, 256 MPa, and 24%. With further increasing the Al_2O_3 addition to 5 wt. % the YS increases to 245 MPa, UTS to 286 MPa, and ductility to 30%. The YS and UTS of the composite drops (to 195 MPa and 221 MPa, respectively) when the reinforcement content reaches 10 wt. %. In summary, the composite reinforced with 5 wt. % Al_2O_3 nanoparticles shows higher YS and UTS compared to the base alloy and composites reinforced with varying percentages of Al_2O_3 nanoparticles considered in this study.

Table 2. Tensile properties of the as-extruded Al-12Si/Al_2O_3 nanoparticle-reinforced composites.

Weight Percent of Al_2O_3 (%)	Yield Strength (MPa)	Ultimate Tensile Strength (MPa)	Elongation (%)
0	198 ± 2	228 ± 2	23 ± 2
2	228 ± 2	256 ± 3	24 ± 2
5	245 ± 2	286 ± 3	30 ± 3
10	195 ± 2	221 ± 2	19 ± 1

Figure 6 shows the tensile fracture surfaces of Al-12Si/Al_2O_3 nanocomposites. It can be observed (Figure 6a) that the fracture mode of the matrix Al-12Si alloy is predominantly ductile with several dimples all over the surface. As shown in Figure 6b, 2 wt. % nano Al_2O_3-reinforced composite also

displays dimples like the matrix Al-12Si alloy, except that the length scale of the dimples are different. Similarly, composites with 5 wt. % Al_2O_3 also show the presence of dimples again at different length scales than the 2 wt. % Al_2O_3 composite and Al-12Si-based alloy. When the Al_2O_3 content is increased to 10 wt. % (Figure 6d), both the number and size of the dimples decrease significantly, leading to a relatively brittle type of failure. Some defects such as cracks and segregation are observed on the fracture surface (along the neighborhood of the Al_2O_3 reinforcement particles), which also limits both the strength and ductility of the composites. The segregation/agglomeration will prevent an effective bonding between the reinforcement and the matrix and may lead to further defects such as cracks in the composites, and these cracks will inevitably leads to a premature failure of the composites. In addition, the agglomeration/clustering of the reinforcement particles can cause the presence of increased porosity in the composites [29].
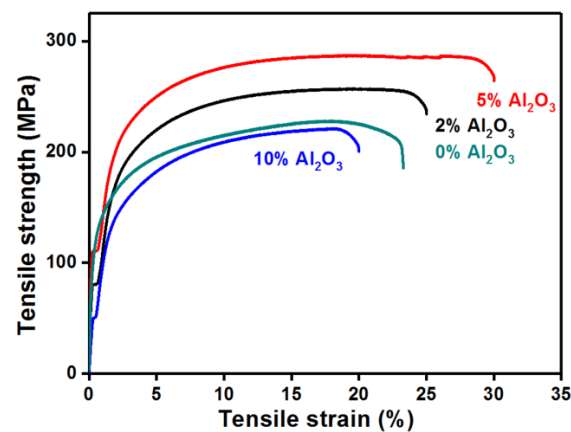

Figure 5. The tensile true stress-true strain curves of Al-12Si/Al_2O_3 nanocomposites produced by the hot extrusion method.
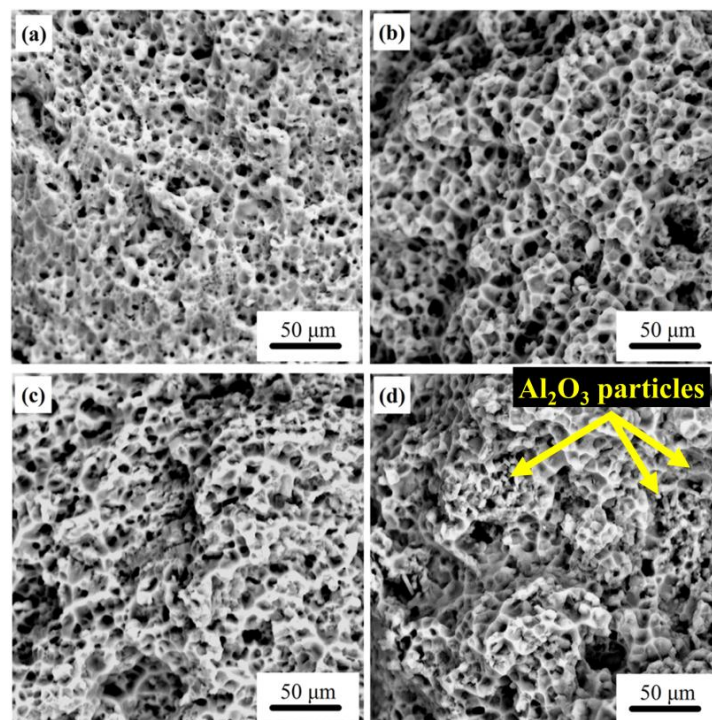

Figure 6. Fracture morphologies of the as-extruded Al-12Si/Al_2O_3 nanocomposites after room temperature tensile tests.

3.3. Strengthening Mechanism

Unlike tensile strength, yield strength usually shows less dependency on the presence of the stress concentrations in the composites. Therefore, yield strength is more representative of the discussion of the strengthening mechanisms [30]. The strengthening mechanisms operating in the Al-12Si/Al$_2$O$_3$ nanocomposites mainly include the load transfer mechanism, Orowan strengthening mechanism, and thermal mismatch enhancement mechanism. These three mechanisms operate simultaneously [31–33]. The most accepted strengthening mechanism is the direct strengthening mechanism, also known as load transfer mechanism. The strengthening of the composites takes place due to the transfer of load from the weaker matrix to the harder reinforcement through their interface, as proposed by Nardon and Prewo [34].

$$\Delta\sigma_{load} = 0.5 f \sigma_m \tag{1}$$

where σ_m is the yield strength of the matrix (MPa), and f is the volume fraction of Al$_2$O$_3$ particles. According to Equation (1), the effect of load transfer is calculated and is given in Table 3. The Orowan strengthening mechanism is very important in metal matrix composites, if the reinforcement particles are fine and the inter-particle spacing is not large. Incremental yield strength of the composite caused by Orowan stress of the Al$_2$O$_3$ particles may be expressed as [35,36]:

$$\Delta\sigma_{orowan} = \frac{0.538 G_m b \sqrt{f}}{d} \ln\frac{d}{2b} \tag{2}$$

where Gm is the shear modulus of the matrix.

$$G_m = G_{Al} V_{Al} + G_{Si} V_{Si} \tag{3}$$

where G_{Al}=27 GPa, G_{Si}= 66.8 GPa, B is the Burgers vector of the matrix, b = ((1.414/2) × 0.286 nm) = 0.202 nm, and d and f are the diameter and volume fraction of Al$_2$O$_3$ particle, respectively. This effect is calculated and the results are given in Table 3. As shown in Table 3, the higher the Al$_2$O$_3$ content, the greater the effect of the Orowan mechanism. When a composite is subjected to thermal changes, then the difference in their coefficients of thermal expansion (CTE) between the matrix and reinforced particles will produce a thermal strain and internal stress state changes. In order to accommodate this thermal mismatch effect, dislocations are generated around reinforced particles within the matrix to reduce the stored energy. The magnitude of thermal strain determines the density of dislocations generated within the composites. The increased dislocation density within the matrix leads to the strengthening of the composite. In this study, the large discrepancy of thermal expansion coefficients between the Al$_2$O$_3$ (7.85 × 10^{-6}/K) and the Al-12Si matrix (20.96 × 10^{-6}/K) generate dislocations in the Al matrix. The improvement in yield strength from thermal mismatch can be calculated using Equation (4) [37–39]:

$$\Delta\sigma_{CTE} = \sqrt{3} a G b \sqrt{\rho_{CTE}} \tag{4}$$

where a is a constant, $a = 1$. ρ_{CTE} is the dislocation density caused by CTE differences, and can be described as follows:

$$\rho_{CTE} = \frac{12 \Delta\alpha \Delta T f}{bd(1-f)} \tag{5}$$

where $\triangle\alpha$ is the CTE difference between the matrix and the reinforcement, $\triangle$T is the temperature difference between the testing temperature and room temperature. This strengthening effect is also shown in Table 3. These strengthening mechanisms are additive, and the total yield strength of the composite could be considered as the sum of different mechanisms rather than the contribution of a single one. In its simplest form, the superposition of the individual strengthening mechanisms may be carried out linearly.

$$\Delta\sigma_C = \Delta\sigma_{Load} + \Delta\sigma_{Orowan} + \Delta\sigma_{CTE} \tag{6}$$

Table 3. Contribution of different strengthening mechanisms on the yield stress of Al-12Si/Al$_2$O$_3$ extruded nanocomposites.

Weight Percent of Al$_2$O$_3$ (%)	$\triangle\sigma_{Load}$ (MPa)	$\triangle\sigma_{Orowan}$ (MPa)	$\triangle\sigma_{CTE}$ (MPa)	$\triangle\sigma_C$ (MPa)
2	1.50	3.85	27.94	33.19
5	4.14	6.13	42.47	52.74
10	6.65	8.75	53.49	68.89

The individual contributions of the described three mechanisms to the yield strength of the composite calculated from Equations (1)–(4) are listed in Table 3 as a function of the weight percentage of Al$_2$O$_3$ nanoparticles. The presented data show that the effect induced by thermal mismatch strengthening ($\triangle\sigma_{CTE}$) makes the largest contribution to the yield strength improvement. The strength increments resulting from the load transfer ($\triangle\sigma_{Load}$) and Orowan strengthening ($\triangle\sigma_{Orowan}$) are very similar and are much lower. Figure 7 shows the variation of experimental YS and the theoretical values calculated using Equation (6). The total improvement from the multiple strengthening mechanisms for yield strength is ~30 MPa and 45 MPa, and the predicted values of the yield strength for the composites are ~33 MPa and 53 MPa, respectively, for the composites with 2 and 5 wt. % Al$_2$O$_3$ addition. This shows that the experimental and theoretical values are very close and hence the strengthening mechanisms based on load sharing, Orowan mechanism, and thermal mismatch strengthening are expected to play a role in these composites. The small discrepancy between the experimental and theoretical values may arise from the defects (such as porosity, agglomeration, and impurities) present in the samples. A large discrepancy was observed for the composite with 10 wt. % Al$_2$O$_3$ as reinforcement, which was mainly caused by the profound agglomeration of the reinforcement in the composite.
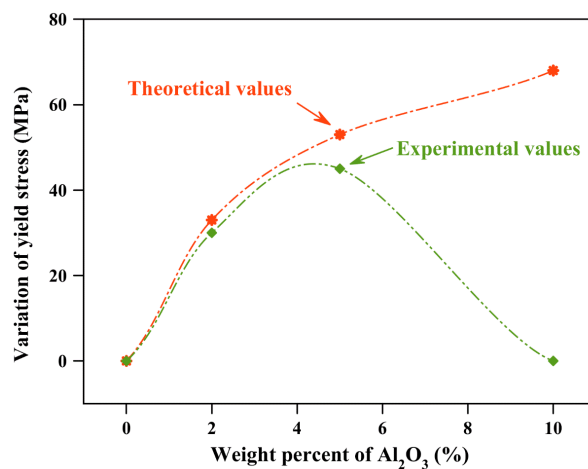
Figure 7. Comparison of the strengthening effect in the as-extruded Al-12Si/Al$_2$O$_3$ nanocomposites between experimental observation and calculated theoretical values.

4. Summary

In this study, Al$_2$O$_3$ nanoparticle-reinforced Al-12Si composites were prepared by hot pressing and subsequent hot extrusion. The microstructure, mechanical properties, and the strengthening mechanisms were investigated in detail. The conclusions are as follows:

(1) The composites reinforced with 2 and 5 wt. % Al$_2$O$_3$ nanoparticles exhibited relatively homogeneous distribution, while the microstructure of the composites with 10 wt. % reinforcement exhibited agglomeration of the Al$_2$O$_3$ particles in the matrix.

(2) The hardness of the composites increased first (for 2 and 5 wt. % reinforcement) and then decreased (for 10 wt. % reinforcement). The strength of the composites also displayed similar trends

to that of the hardness. The maximum values were obtained for the composites with 5 wt. % Al_2O_3. The YS, UTS, and the elongation were 244 MPa, 286 MPa, and ~30%, respectively, with 5 wt. % Al_2O_3 addition, which showed an increase to about ~23%, 26%, and 30%, respectively, compared with the Al-12Si matrix alloy.

(3) The strengthening mechanism analysis shows that the yield strength of the composites increased mostly because of the thermal mismatch enhancement mechanism compared to the other two strengthening mechanisms (load transfer and Orowan strengthening).

Author Contributions: Yandong Jia and Prashanth Konda Gokuldoss formulated the idea. ZhiShui Yu and Jian Zhao helped with the literature survey. Pan Ma, Shanglei Yang and Chonggui Li carried out the experiments, Pan Ma wrote the paper and Prashanth Konda Gokuldoss supervised the research.

Conflicts of Interest: The authors declare no conflict of interest.

References

1. Scudino, S.; Liu, G.; Prashanth, K.G.; Bartusch, B.; Surreddi, K.B.; Murty, B.S.; Eckert, J. Mechanical properties of Al-based metal matrix composites reinforced with Zr-based glassy particles produced by powder metallurgy. *Acta Mater.* **2009**, *57*, 2029–2039. [CrossRef]
2. Bodunrin, M.O.; Alaneme, K.K.; Chown, L.H. Aluminium matrix hybrid composites: A review of reinforcement philosophies; mechanical, corrosion and tribological characteristics. *J. Mater. Res. Technol.* **2015**, *4*, 434–445. [CrossRef]
3. Hunt, W.; Herling, D.R. Aluminum Metal Matrix Composites. *Adv. Mater. Process.* **2004**, *162*, 39–44.
4. Wang, Z.; Prashanth, K.G.; Scudino, S.; Chaubey, A.K.; Sordelet, D.J.; Zhang, W.W.; Li, Y.Y.; Eckert, J. Tensile properties of Al matrix composites reinforced with in-situ devitrified $Al_{84}Gd_6Ni_7Co_3$ glassy particles. *J. Alloy. Compd.* **2014**, *586*, S419–S422. [CrossRef]
5. Prashanth, K.G.; Scudino, S.; Chaubey, A.K.; Lober, L.; Wang, P.; Attar, H.; Schimansky, F.; Pyczak, F.; Eckert, J. Processing of Al-12Si–TNM composites by selective laser melting and evaluation of compressive and wear properties. *J. Mater. Res.* **2016**, *31*, 55–65. [CrossRef]
6. Wang, Z.; Tan, J.; Sun, B.A.; Scudino, S.; Prashanth, K.G.; Zhang, W.W.; Li, Y.Y.; Eckert, J. Fabrication and mechanical properties of Al-based metal matrix composites reinforced with $Mg_{65}Cu_{20}Zn_5Y_{10}$ metallic glass particles. *Mater. Sci. Eng. A* **2014**, *600*, 53–58. [CrossRef]
7. Mazahery, A.; Abdizadeh, H.; Baharvandi, H.R. Development of high- performance A356/nano-Al_2O_3 composites. *Mater. Sci. Eng. A* **2009**, *518*, 61–64. [CrossRef]
8. Tjong, S.C. Novel nanoparticle-reinforced metal matrix composites with enhanced mechanical properties. *Adv. Eng. Mater.* **2007**, *9*, 639–652. [CrossRef]
9. Habibnejad-Korayem, M.; Mahmudi, R.; Poole, W.J. Enhanced properties of Mg-based nano-composites reinforced with Al_2O_3 nano-particles. *Mater. Sci. Eng. A* **2009**, *519*, 198–203. [CrossRef]
10. Shehata, F.; Fathy, A.; Abdelhameed, M.; Moustaf, S.F. Preparation and properties of Al_2O_3 nanoparticle reinforced copper matrix composites by in situ processing. *Mater. Des.* **2009**, *30*, 2756–2762. [CrossRef]
11. Karbalaei Akbari, M.; Mirzaee, O.; Baharvandi, H.R. Fabrication and study on mechanical properties and fracture behavior of nanometric Al_2O_3 particle- reinforced A356 composites focusing on the parameters of vortex method. *Mater. Des.* **2013**, *46*, 199–205. [CrossRef]
12. Su, H.; Gao, W.L.; Feng, Z.H.; Lu, Z. Processing, microstructure and tensile properties of nano-sized Al_2O_3 particle reinforced aluminum matrix composites. *Mater. Des.* **2012**, *36*, 590–596. [CrossRef]
13. Sajjadi, S.A.; Ezatpour, H.R.; Beygi, H. Microstructure and mechanical properties of Al-Al_2O_3 micro and nano composites fabricated by stir casting. *Mater. Sci. Eng. A* **2011**, *528*, 8765–8771. [CrossRef]
14. Sajjadi, S.A.; Ezatpour, H.R.; Torabi Parizi, M. Comparison of microstructure and mechanical properties of A356 aluminum alloy/Al_2O_3 composites fabricated by stir and compo-casting processes. *Mater. Des.* **2012**, *34*, 106–111. [CrossRef]

15. Chou, S.N.; Huang, J.L.; Lii, D.F.; Lu, H.H. The mechanical properties of Al_2O_3/aluminum alloy A356 composite manufactured by squeeze casting. *J. Alloys Compd.* **2006**, *419*, 98–102. [CrossRef]

16. Amirkhanlou, S.; Niroumand, B. Effects of reinforcement distribution on low and high temperature tensile properties of $Al356/SiC_p$ cast composites produced by a novel reinforcement dispersion technique. *Mater. Sci. Eng. A* **2011**, *528*, 7186–7195. [CrossRef]

17. Karbalaei Akbari, M.; Baharvandi, H.R.; Mirzaee, O. Fabrication of nano-sized Al_2O_3 reinforced casting aluminum composite focusing on preparation process of reinforcement powders and evaluation of its properties. *Compos. Part B.* **2013**, *55*, 426–432. [CrossRef]

18. Li, S.F.; Sunb, B.; Imaia, H.; Mimotob, T.; Kondoha, K. Powder metallurgy titanium metal matrix composites reinforced with carbon nanotubes and graphite. *Compos. Part A* **2013**, *48*, 57–66. [CrossRef]

19. Kallip, K.; Kishore Babu, N.; AlOgab, K.A.; Kollo, L.; Maeder, X.; Arroyo, Y.; Leparoux, M. Microstructure and mechanical properties of near net shaped aluminium/alumina nanocomposites fabricated by powder metallurgy. *J. Alloys Compd.* **2017**, *714*, 133–143. [CrossRef]

20. Prashanth, K.G.; Murty, B.S. Production, kinetic study and properties of Fe-based glass and its composites. *Mater. Manuf. Processes.* **2010**, *25*, 592–597. [CrossRef]

21. Wang, Z.; Tan, J.; Scudino, S.; Sun, B.A.; Qu, R.T.; He, J.; Prashanth, K.G.; Zhang, W.W.; Li, Y.Y.; Eckert, J. Mechanical behavior of Al-based matrix composites reinforced with $Mg_{58}Cu_{28.5}Gd_{11}Ag_{2.5}$ metallic glass. *Adv. Powder technol.* **2014**, *25*, 635–639. [CrossRef]

22. Marko, D; Prashanth, K.G.; Scudino, S.; Wang, Z.; Ellendt, N.; Uhlenwinkel, V.; Eckert, J. Al-based metal matrix composites reinforced with $Fe_{49.9}Co_{35.1}Nb_{7.7}B_{4.5}Si_{2.8}$ glassy powder: Mechanical behavior under tensile loading. *J. Alloys Compd.* **2014**, *615*, S382–S385. [CrossRef]

23. Tabandeh Khorshid, M.; Jenabali Jahromi, S.A.; Moshksar, M.M. Mechanical properties of tri-modal Al matrix composites reinforced by nano- and submicron sized Al_2O_3 particulates developed by wet attrition milling and hot extrusion. *Mater. Des.* **2010**, *31*, 3880–3884. [CrossRef]

24. Razavi, H.Z.; Hafizpour, H.R.; Simchi, A. An investigation on the compressibility of aluminum/nano-alumina composite powder prepared by blending and mechanical milling. *Mater. Sci. Eng. A* **2007**, *454–455*, 89–98. [CrossRef]

25. Prashanth, K.G.; Scudino, S.; Klauss, H.J.; Surreddi, K.B.; Löber, L.; Wang, Z.; Chaubey, A.K.; Kühn, U.; Eckert, J. Microstructure and mechanical properties of Al-12Si produced by selective laser melting: Effect of heat treatment. *Mater. Sci. Eng. A* **2014**, *590*, 153–160. [CrossRef]

26. Suryawanshi, J.; Prashanth, K.G.; Scudino, S.; Eckert, J.; Prakash, O.; Ramamurty, U. Simultaneous enhancements of strength and toughness in an Al-12Si alloy synthesized using selective laser melting. *Acta Mater.* **2016**, *115*, 285–294. [CrossRef]

27. Prashanth, K.G.; Scudino, S.; Eckert, J. Defining the tensile properties of Al-12Si parts produced by selective laser melting. *Acta Mater.* **2017**, *126*, 25–35. [CrossRef]

28. Prashanth, K.G.; Debalina, B.; Wang, Z.; Gostin, P.; Gebert, A.; Calin, M.; Kühn, U.; Kamaraj, M.; Scudino, S.; Eckert, J. Triobological and corrosion properties of Al-12Si produced by selective laser melting. *J. Mater. Res.* **2014**, *29*, 2044–2054. [CrossRef]

29. Li, C.D.; Wang, X.J.; Liu, W.Q.; Wu, K.; Shi, H.L.; Ding, C.; Hu, X.S.; Zheng, M.Y. Microstructure and strengthening mechanism of carbon nanotubes reinforced magnesium matrix composite. *Mater. Sci. Eng. A* **2014**, *597*, 264–269. [CrossRef]

30. Zhang, D.; Zhan, Z. Preparation of graphene nanoplatelets-copper composites by a modified semi-powder method and their mechanical properties. *J. Alloys Compd.* **2016**, *654*, 226–233. [CrossRef]

31. Li, M.Q.; Zhai, H.X.; Huang, Z.Y.; Liu, X.H.; Zhou, Y.; Li, S.B.; Li, C.W. Tensile behavior and strengthening mechanism in ultrafine $TiC_{0.5}$ particle reinforced Cu-Al matrix composites. *J. Alloys Compd.* **2015**, *628*, 186–194. [CrossRef]

32. Park, J.G.; Keum, D.H.; Lee, Y.H. Strengthening mechanisms in carbon nanotube-reinforced aluminum composites. *Carbon.* **2015**, *95*, 690–698. [CrossRef]

33. Bisht, A.; Srivastava, M.; Manoj Kumar, R.; Lahir, I.; Lahiri, D. Strengthening mechanism in graphene nanoplatelets reinforced aluminum composite fabricated through spark plasma sintering. *Mater. Sci. Eng. A* **2017**, *695*, 20–28. [CrossRef]

34. Nardone, V.C.; Prewo, K.M. On the strength of discontinuous silicon carbide reinforced aluminum composites. *Scripta Metall.* **1986**, *20*, 43–48. [CrossRef]

35. Bakshi, S.R.; Agarwal, A. An analysis of the factors affecting strengthening in carbon nanotube reinforced aluminum composites. *Carbon* **2011**, *49*, 533–544. [CrossRef]

36. Ma, F.C.; Zhou, J.J.; Liu, P.; Li, W.; Liu, X.K.; Pan, D.; Lu, W.J.; Zhang, D.; Wu, L.Z.; Wei, X.Q. Strengthening effects of TiC particles and microstructure refinement in insitu TiC-reinforced Ti matrix composites. *Mater. Charact.* **2017**, *127*, 27–34. [CrossRef]

37. Sree Manu, K.M.; Arun Kumar, S.; Rajan, T.P.D.; Riyas Mohammed, M.; Pai, B.C. Effect of alumina nanoparticle on strengthening of Al-Si alloy through dendrite refinement, interfacial bonding and dislocation bowing. *J. Alloys Compd.* **2017**, *712*, 394–405. [CrossRef]

38. Li, J.; Liu, B.; Fang, Q.H.; Huang, Z.W.; Liu, Y.W. Atomic-scale strengthening mechanism of dislocation-obstacle interaction in silicon carbide particle- reinforced copper matrix nanocomposites. *Ceram. Int.* **2017**, *43*, 3839–3846. [CrossRef]

39. Zhao, X.; Lu, C.; Tieu, A.K.; Pei, L.Q.; Zhang, L.; Cheng, K.Y.; Huang, M.H. Strengthening mechanisms and dislocation processes in <111> textured nanotwinned copper. *Mater. Sci. Eng. A* **2016**, *676*, 474–486. [CrossRef]